Mon. Not. R. Astron. Soc. **000**, 000–000 (0000) Printed 16 January 2014 (MN LATEX style file v2.2)

Fluorescent Lyman-alpha Emission from Gas Near a QSO at Redshift 4.28

Paul J. Francis[1,2⋆] and Sunsanee McDonnell[1]
[1] *Research School of Astronomy and Astrophysics, the Australian National University, Canberra 0200, Australia*
[2] *Joint Appointment with the Department of Physics, Faculty of Science, the Australian National University*

arXiv:astro-ph/0605477v1 19 May 2006

16 January 2014

ABSTRACT

We use integral field spectroscopy with the Gemini North Telescope to detect probable fluorescent Lyα emission from gas lying close to the luminous QSO PSS 2155+1358 at redshift 4.28. The emission is most likely coming not from primordial gas, but from a multi-phase, chemically enriched cloud of gas lying about 50 kpc from the QSO. It appears to be associated with a highly ionised associated absorber seen in the QSO spectrum. With the exception of this gas cloud, the environment of the QSO is remarkably free of neutral hydrogen. We also marginally detect Lyα emission from a foreground sub-Damped-Lyα absorption-line system.

Key words: Intergalactic medium — quasars: absorption-lines — quasars: individual: PSS 2155+1358 — galaxies: high-redshift

1 INTRODUCTION

Flows of gas play a crucial role in galaxy formation – both the infalling primordial gas from which galaxies ultimately form, and outflows which enrich the intergalactic medium and regulate galaxy formation. Much attention has recently been placed on one possible way of directly observing this gas: Lyα fluorescence. The idea, originally proposed by Hogan & Weymann (1987) is that the plentiful Ultraviolet (UV) radiation in the high redshift universe will be absorbed by any neutral gas, and some fraction of the incident ionising photons will be re-radiated as Lyα photons (Gould & Weinberg 1996; Bunker, Marleau & Graham 1998; Francis et al. 2001; Francis & Bland-Hawthorn 2004; Cantalupo et al. 2005).

This fluorescent Lyα emission will be brightest where the UV radiation is strongest: close to luminous QSOs. Haiman & Rees (2001) and Alam & Miralda-Escudé (2002) predicted that QSOs with sufficiently high redshifts should be surrounded by halos of Lyα emission, as the UV flux from the QSO causes the still infalling primordial gas to fluoresce. The predicted intensity of this flux is, however, very dependent upon assumptions on how the gas is clumped.

The observational picture is currently confusing. It has long been established that many high redshift radio sources, both QSOs and radio galaxies, have bright Lyα emission coming from around them (e.g. Heckman et al. 1991; Bremer et al. 1992; Hu, McMahon & Egami 1996; Venemans et al. 2002), but this may be caused by the radio jets, winds or cooling flows, rather than fluorescence. Luminous extended Lyα nebulae ("blobs") are fairly common at high redshifts, but not obviously associated with QSOs: they may be caused by cooling flows, superwinds or photoionisation by concealed AGNs (e.g.. Furlanetto et al. 2003; Matsuda et al. 2004; Colbert et al. 2006, and refs therein).

There are less data available for radio-quiet QSOs. Damped Lyα absorption-line systems that lie close to the QSO redshift have been detected in possible fluorescent emission in a few cases (Møller & Warren 1993; Møller, Warren & Fynbo 1998). More recently, probable fluorescent emission was seen from another absorption system, but this time the absorber was 380 kpc away, in front of a different QSO (Adelberger et al. 2006). Francis & Bland-Hawthorn (2004) failed to detect any fluorescent emission around a QSO, and indeed claimed that the presence of the QSO was suppressing even the normal background population of Lyα emitting galaxies. On the other hand, Weidinger, Møller & Fynbo (2004) detected Lyα fuzz close to a $z = 3$ QSO which they modeled as a spherical infalling halo of primordial gas. Bunker et al. (2003) found spectacularly bright Lyα fuzz, with a high velocity dispersion, around a QSO at redshift 4.46. Barkana & Loeb (2003) suggest that evidence for infalling primordial gas around high redshift QSOs can be seen in the detailed profiles of the QSO emission line.

It is thus becoming clear that fluorescent Lyα can be detected with current telescope facilities, but on the basis of the extremely small number statistics available to date, its

⋆ E-mail: pfrancis@mso.anu.edu.au (PJF)

properties appear to be heterogeneous. A larger sample size would clearly be useful. In this paper we contribute to this effort, searching for fluorescent emission near the brightest accessible QSO with a redshift above four: PSS 2155+1358, at redshift 4.28.

Previous detections of fluorescent Lyα have used either long-slit spectroscopy (e.g. Bunker et al. 2003) or narrow-band imaging (eg. Francis & Bland-Hawthorn 2004). Long-slit spectroscopy has the disadvantage that the slit may not be at the right orientation to catch any emission. Narrow-band imaging is only possible if the QSO redshift is known with high precision, which is not usually the case. In this paper we try a different approach: integral field unit (IFU) spectroscopy.

We assume a cosmology with $H_0 = 70\mathrm{km\ s^{-1}Mpc^{-1}}$, $\Omega_{\mathrm{matter}} = 0.3$ and $\Omega_\Lambda = 0.7$ throughout this paper.

2 OBSERVATIONS AND DATA REDUCTION

The QSO PSS 2155+1358 was observed with the integral field unit of the Gemini Multi-Object Spectrograph (GMOS) on the Gemini North Telescope. The B600 grating was used in two-slit mode, giving a spectral resolution of $R = 1688$, over the $5{\times}7''$ IFU field of view. The r_G0303 filter was used to limit the wavelength range to $562 - 698$nm and hence prevent spectra from the two slits from overlapping. A central wavelength of 625nm was used, with some dithering in the spectral direction between frames to eliminate chip gaps.

Observations were obtained in queue mode. Observations were taken on 2004 August 14, September 11 and September 14, in clear weather conditions and with seeing varying between 0.7 and 0.9 arcsec. A total exposure time of 6 hours was obtained.

The data were reduced using the Gemini IRAF (Image Reduction and Analysis) package. Standard settings were used to flat field and bias subtract the frames, extract the spectra, wavelength calibrate and sky subtract the spectra, and assemble them into a data cube. There was a problem with the wavelength calibration, due to a (now rectified) issue with the grating mounts. As a result, the absolute wavelength calibration of each frame, based on arc lines, was out by a small amount: different frames had to be aligned using absorption-lines in the spectra before co-addition. We used sky lines to make sure that the wavelength calibration was at least self-consistent between all the fibres in a give slit. The final co-added data cube was put on a correct wavelength scale by comparing the absorption line centroids with those measured in an independent higher resolution spectrum (§ 3.1). The product was a data cube with 0.2 arcsec spatial pixels and 0.092nm spectral pixels.

Sky subtraction used a separate $5{\times}3.5''$ sky region, one arcmin from the QSO. This subtraction (as performed by the Gemini IRAF package) left a flat residual, probably due to scattered light: this residual was weakly wavelength dependent but differed considerably between the two slits. This led to a wavelength dependent step in the background level between the left and right hand sides of any image slice through the data cube. As the QSO sat exactly on the boundary between the two halves, this would have been disastrous for point spread function subtraction if it had not been corrected. An IRAF script was written to perform this correction. For each spatial slice through the data cube, the top and bottom three pixels in each column were medianed, and this median subtracted from the whole column.

2.1 Searching for diffuse line emission

We first searched for diffuse line emission which might fill the whole IFU field of view, as would be seen if the QSO was embedded, for example, in a giant Lyα blob. For this measurement, the scattered light correction mentioned in the previous section was not used.

In each $5 \times 7''$ spatial slice, we averaged the two ends: the first and last $5 \times 1''$ regions, which were free of QSO light. The average of these two regions was plotted, looking for narrow spikes.

The largest spikes had an amplitude (average, over both $5 \times 1''$ regions) of $1.2 \times 10^{-18}\mathrm{erg\ cm^{-2}s^{-1}arcsec^{-2}}$ over a three spectral pixel (1300 km s^{-1}) velocity range. This is a conservative upper limit: over the majority of the spectrum (away from the rare strong sky lines) the limit is a factor of three better.

2.2 Searching for compact emission

We next searched the data cube for any compact emission-line sources. This was done both with and without subtraction of the QSO point spread function.

Point spread function (PSF) subtraction was done using an IRAF script as follows. For each spectral slice through the data cube, a separate point spread function was calculated. It was formed from the median of all the spectra slice images in the velocity ranges $-4300{:}{-}1300$ and $+1300{:}{+}4300\mathrm{km\ s^{-1}}$. Images in which the QSO flux was very low due to an absorption line were excluded from this median. The PSF image thus constructed was scaled to have the correct flux in the central $0.6 \times 0.6''$ region of the QSO, and subtracted from the spectral slice image. This procedure worked very well in general, giving PSF subtraction errors typically smaller than the background noise. Several other PSF subtraction techniques were used, but gave poorer results. These other techniques were, however, used as a check on any objects discovered.

Unfortunately, a sub-set of image slices had errors considerably above the background noise, for a variety of reasons:

- Wavelength shifts between the two halves of the image. It turned out that the wavelength solution for the two halves of the image (deriving from the two GMOS slits) was different, albeit only at the sub-pixel level. This introduced artifacts in the PSF subtracted image where the gradient of the QSO spectrum was steep, typically at the edges of narrow absorption lines. Unfortunately our spectral sampling was not sufficient to fully remove it. It produced, however, an easily recognised characteristic symmetrical left-right pattern, and only occurred at the edge of strong narrow absorption lines.
- Chip gaps. The GMOS camera uses a three-CCD mosaic, which produced gaps in the wavelength coverage of any individual spectrum. We observed at four different central wavelengths, ensuring that we had at least three quarters of

our data at any given wavelength. As the seeing differed between the different nights' data, however, the seeing width in the co-added data-cube varied depending which nights data were used at a given wavelength. This led to strong residuals in the PSF subtraction near the edges of any of the regions affected by a chip gap. Once again, this produced a very characteristic pattern (a positive or negative ring in the subtracted image) and it was easy to check that such rings were indeed produced by a chip gap.

• Other glitches. There were occasional glitches away from the QSO position, due to cosmic ray hits, defects in the CCDs and problems in the spectrum extraction software. These were mercifully rare, and typically easy to recognise because they affected either a region smaller than the PSF, or a whole row or column in the data. A disadvantage of fibre IFU designs such as GMOS is that the mapping between pixels in the raw data and those in the final data cube is very complex and not one-to-one, making it extremely time-consuming checking the origin of glitches such as these.

For all these reasons, it did not prove possible to do an automated search for line emission. Instead, the whole cube was eyeballed independently by the two authors, and lists of candidate emission-line objects assembled. These candidates were then checked in detail to eliminate the various glitches. Errors were estimated from the size of the largest candidate objects for which it was not possible to confidently decide whether they were glitches or not. This error limit typically a factor of ~ 2 greater than the (3σ) sky noise limit.

Our detection limit was estimated by inserting artificial point-sources into various image slices, carrying out the point spread function subtraction and seeing if they were obviously seen, and easily distinguished from the various artifacts. As shown in Fig 1, our sensitivity to point sources is a strong function of how far they are in projection from the QSO.

3 RESULTS

The QSO spectrum is shown in Fig 2, and shows a strong Lyα line peaking at around 642 nm, and many absorption lines. The observed QSO flux is 181 μJy at 660nm.

Only one significant Lyα emitter was discovered, at 641.97nm (We defer discussion of a second, marginally significant emitter to § 5). This emission-feature can be clearly seen in each night's data independently, so we regard the detection as secure.

The 641.97nm line emission comes from $0.8''$ east of the QSO. It is spectrally unresolved (Fig 5) with a line width (full width at half maximum height, FWHM) of $\sim$ 0.3nm (140km s^{-1}). A flux of 1.5×10^{-17}erg cm^{-2}s^{-1} was measured by point-spread function fitting of the QSO PSF subtracted image. Note that this is a lower limit on the true flux, as any flux overlapping the centre of the QSO image will have been removed by the QSO PSF subtraction. No continuum emission is detected at this location: this allows us to place a lower limit of $\sim$ 10nm (observed frame) on the equivalent width of the line.

The line lies at the peak of the broad QSO Lyα emission-line, at almost the same wavelength as a strong narrow Lyα absorption-line system (Fig 4). The emission peak is offset by 45 ± 30km s^{-1} (1σ uncertainty) to the blue of the absorption-line centroid. The emitter is not an artefact of the wavelength calibration problem at the edge of strong absorption-lines, noted in § 2.1: it lies on the flat part of the QSO spectrum near the base of the absorber, where this artefact is not important.

Table 1. Upper limits on the absorption column density of each absorbing component.

Ion	$\log_{10}(ColumnDensity)$, cm^{-2}
N III	13.8
N II	12.5
N I	14.5
C III	13.3
C II	12.8
C I	12.5
Si IV	12.5
Si II	11.9
Si I	13.3
Fe III	14.3
Fe II	13.2
Al II	11.5
Ni II	12.5
S I	13.5
O I	13.5

3.1 Absorption Line

What are the properties of this absorption-line, which lies at the same redshift as the Lyα emitter? Celine Péroux kindly made available to us a spectrum of QSO PSS 2155+1358 obtained with the Ultra-Violet Echelle Spectrograph (UVES) on the Very Large Telescope (VLT). This spectrum is described in Dessauges-Zavadsky et al. (2003). This spectrum was used to investigate the properties of the absorption-line at the same wavelength as the z=4.2793 emitter.

The line is clearly seen in multiple Lyman-series lines, allowing an accurate neutral hydrogen column density of 4.68×10^{15}cm^{-2} to be measured. The line width parameter $b = 32$km s^{-1}.

The line is also detected in N V and C IV, where it breaks up into at least three sub-components each with a velocity width of no greater than 10km s^{-1} (Fig 6), spread over a 40km s^{-1} velocity range. We fit the absorption with a three-sub-component model: component a is at a vacuum heliocentric redshift of z=4.2806, component b at z=4.2809 and component c at z=4.2812.

Column densities were measured interactively using the XVOIGT program (Mar and Bailey 1995) The C IV column densities are 6.3, 9.1 and 8.5×10^{13}cm^{-2} for components a, b and c respectively. For N V, component a has a column density 6.31×10^{13}cm^{-2}, while the combined column density of components b and c is 1.16×10^{14}cm^{-2}. Upper limits on the column density of each individual component in other transitions are given in Table 1.

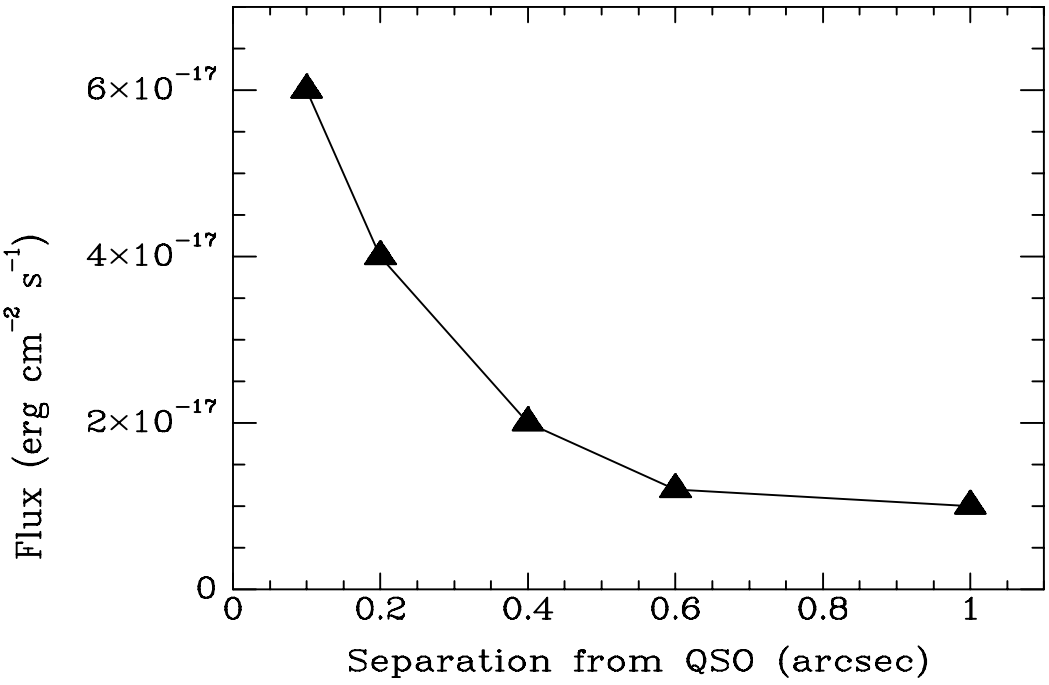


Figure 1. Detection limits for spectrally unresolved point source line emitters, as a function of distance from the QSO. This curve was determined near the peak of the QSO Lyα emission line: sensitivities will be better a wavelengths where the QSO is fainter.

4 DISCUSSION

4.1 Is the line Lyα?

Is this emission line due to Lyα emission at redshift 4.2793, or could it be emission from a foreground galaxy, in a different line? The detected line is too narrow to be [O II] (372.7nm), as we would have easily resolved the doublet. The main possibilities are thus Hβ and the [O III] doublet. If it were any of these lines, we might have expected to see one of the others. The expected wavelengths for all the various possibilities were checked and nothing was seen.

We can put a conservative lower limit on the equivalent width of the line of 10nm. This is quite normal for Lyα emitting galaxies, but would be extremely high for a foreground galaxy (eg. Francis, Nelson & Cutri 2004).

We therefore conclude that the line is most likely Lyα. Further evidence for this hypothesis comes from the probability argument in § 4.3.

4.2 What is the QSO's Redshift?

To work out whether the Lyα emitter we saw is associated with the QSO, we need to know the QSO redshift. Péroux et al. (2001) estimated the QSO redshift by fitting Gaussians to the peak of the Lyα, Si IV/O IV (140nm) and C IV (154.8nm) lines. Their data consisted of a spectrum with a relatively low resolution and signal-to-noise ratio. The results were discrepant: z=4.285 from Lyα, 4.269 from Si IV/O IV and a much lower value of 4.216 from C IV. The discrepancy was unsurprising, as all three lines were strongly affected by absorption-line systems.

We used the UVES spectrum to better determine the redshift. Its higher resolution and signal-to-noise ratio allowed us to clearly see the continuum between the absorption lines. From this spectrum, we see that the Lyα emission line really does have quite a sharp peak, and that the downturn below 639nm is real and not due to absorption. Using this peak wavelength, we get a redshift estimate of 4.28 ± 0.02. Measuring a redshift from the metal lines proved to be harder, as both have extremely broad, flat profiles, without a well defined peak. Our best estimate is 4.26 ± 0.04 for Si IV/O IV, and 4.25 ± 0.04 for C IV.

The results are thus still discrepant, albeit all overlapping within their respective error bars. Francis et al. (1992) showed that CIV is systematically blue-shifted in radio-quiet QSOs, and that this blueshift is strongest when the line is broadest and has a flat top. The narrow core of Lyα, if present, seems to be a more reliable redshift indicator, provided you have enough spectral resolution to measure the true continuum shape through the Lyα forest absorption.

Another clue to the redshift comes from a series of associated C IV absorption lines, covering a range of redshift, with the highest at z=4.2793. Unless this gas is infalling rapidly into the QSO, this places a lower limit on the true redshift.

Taken together, we thus prefer the higher redshift measured in Lyα: $z_{\rm QSO} = 4.28 \pm 0.02$.

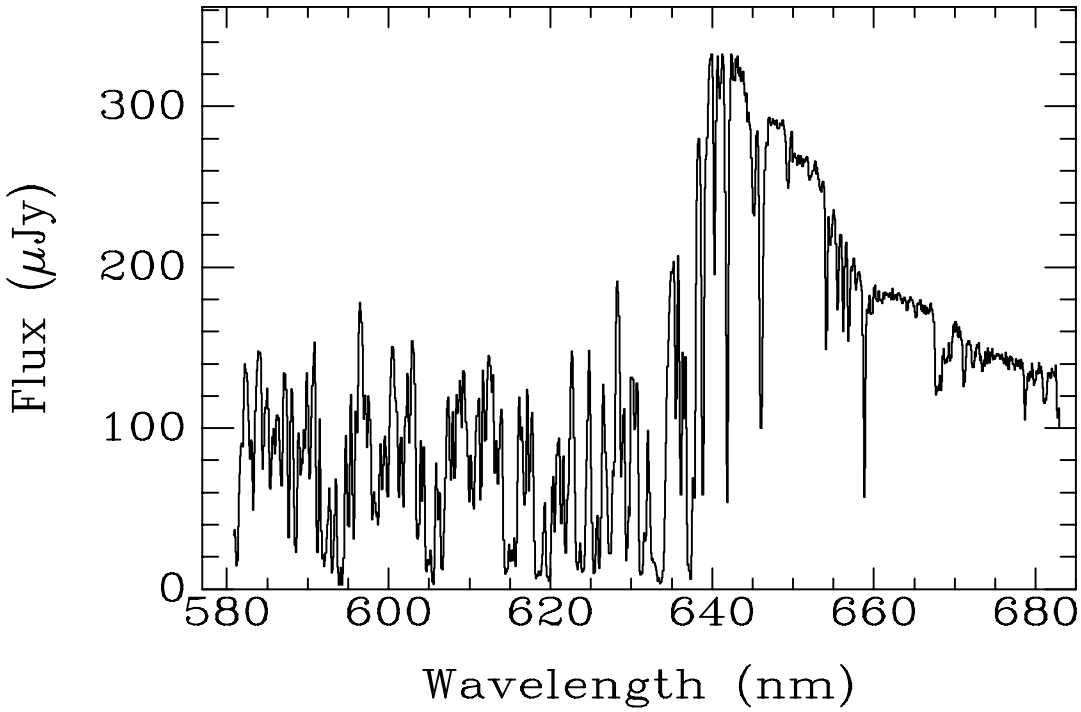


Figure 2. Spectrum of QSO PSS 2155+1358, extracted from the GMOS data cube.

4.3 Is the Emitter at the QSO's Redshift?

In this section we argue that the odds of detecting a Lyα emitter by chance close in both redshift and projected distance to the QSO are small. We therefore conclude that the emitter we saw is indeed physically close to the QSO.

Hu, Cowie & McMahon (1998) measure the surface density of Lyα emitters at z=4.5 down to a flux limit close to ours. Using their surface density, we would only have expected to find ~ 0.08 emitters in our whole data cube. The odds of seeing one by chance within one projected arcsec of the QSO is $< 1\%$. And the odds of finding one that is also within the redshift range 4.28 ± 0.02 is $< 0.07\%$. We can also do the probability calculation internally to our data, by noting that no Lyα emitters were found in the outer regions of our data cube (20 square arcsec, $\Delta z = 0.82$) while one was seen within one arcsec of the QSO in the redshift range 4.28 ± 0.02. The ratio of volumes is thus 128:1.

It is thus quite unlikely that we would have found our one source so close to the QSO by chance. We therefore conclude that the probability of finding a Lyα emitter is enhanced close to the QSO, and that the QSO and emitter really lie close to each other.

4.4 Are the Emitter and Absorber Connected?

The wavelength of our Lyα emitter lies within 45km s^{-1} (0.1 nm) of the wavelength of an associated absorption-line system in the QSO spectrum. Is this coincidence, or could the two be physically connected?

How likely is such a coincidence? Consider a random Lyα emitter, which lay at a redshift within our uncertainty on the redshift of the QSO (4.28 ± 0.02), and which we would thus consider to be associated with the QSO. There are two strong absorption-lines within this redshift interval (Fig 4). The odds of a random emitter lying within 0.1 nm of one of these absorbers is 8%. This assumes no wavelength dependence in our sensitivity limit. In practice, we are more sensitive where the QSO spectrum is weaker, but our emitter is strong enough to have been detected regardless of the QSO flux at that wavelength.

This number is small, but not small enough to rule out the possibility that the redshift match between absorber and emitter is coincidence. We conclude that while it is quite likely that the absorber and emitter are connected, this has not been proved.

4.5 Physical Properties of the Gas

We have concluded that the Lyα emitter at $z = 4.2793$ lies close to the QSO, and may well be connected with the gas producing the absorption line 45km s^{-1} further to the red. What can we learn about the physical properties of this absorber?

For our adopted cosmology, the Lyα emitting cloud is spectrally unresolved (FWHM < 150km s^{-1}), spatially either marginally resolved or unresolved (size $< 5 \times 5$kpc), and has a luminosity of 2.6×10^{42}erg s^{-1}: more if we've over-done the PSF subtraction. It lies at a projected distance of 5kpc from the QSO

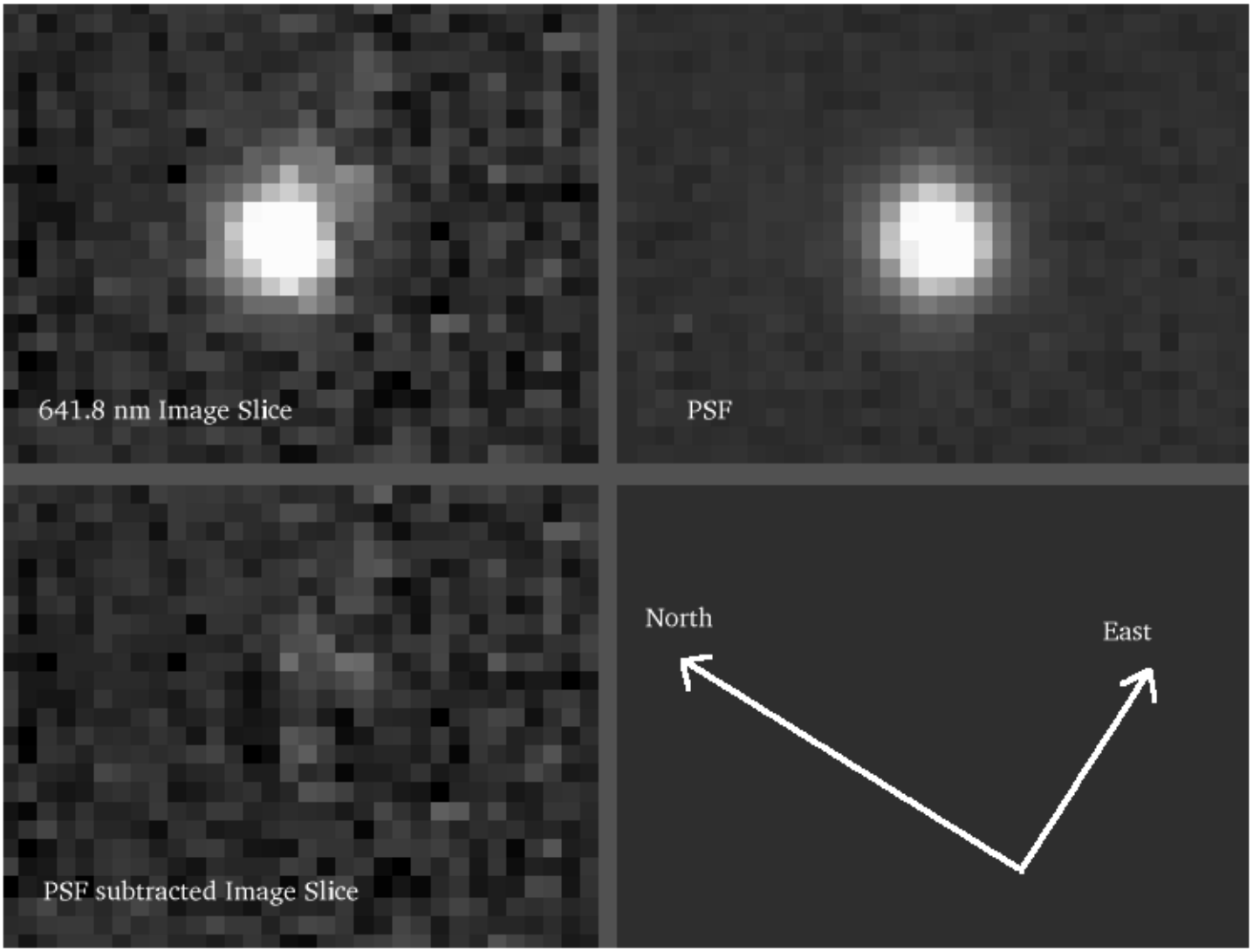


Figure 3. The candidate Lyα emitter at redshift 4.2793. The top left panel shows a single spatial slice through the data cube at 630.00nm wavelength. The point spread function generated from other slices near this wavelength is shown in the top right panel. The bottom left panel shows the PSF subtracted image. The emitter is above and to the right of the QSO. Each image is 7″ wide and 5″ high. Upwards in the images corresponds to 50° east of north on the sky.

Let us first assume that the cloud is 4×4 kpc in size, and optically thick at the Lyman-limit. Following the method in Francis & Bland-Hawthorn (2004), we can estimate the fluorescent Lyα emission that the incident QSO flux will induce in it, as a function of its (proper) distance from the QSO. If it were $\sim$ 5kpc from the QSO, its predicted luminosity would be $\sim$ 400 times greater than that observed.

There are several ways to explain its faintness:

- The cloud, while seen close in projection to the QSO, is actually $\sim$ 100kpc in-front of or behind the QSO, and thus exposed to less ionizing radiation.
- The cloud is much smaller than the seeing disk: less than 1 kpc on a side.
- The cloud, while large, is mostly optically thin, with only a small filling factor of optically thick gas reprocessing the QSO flux.
- Dust or optical depth effects suppress the Lyα flux.
- The QSO could have been much fainter a few thousand years ago: due to light travel time, the cloud luminosity reflects the QSO luminosity in the past.

If, however, we assume that the emitting gas is connected with the absorption-line system, we can deduce much more about its physical conditions, and rule out several of these possibilities.

Firstly, if the emitting and absorbing gas come from different parts of the same cloud, that gives us a cloud size of at least 5kpc. Secondly, the absorption consists of three sub-clumps, spread over $\sim$ 40km s^{-1}. If the cloud really had a very small filling factor of these absorbing sub-clumps, the odds of finding three along the QSO sight-line would have been small. It is therefore likely that the filling factor of sub-clumps is such that most sight-lines would intersect at least one. Thirdly, the measured neutral hydrogen column is too small to make the clouds optically thick in Lyα, and the fact

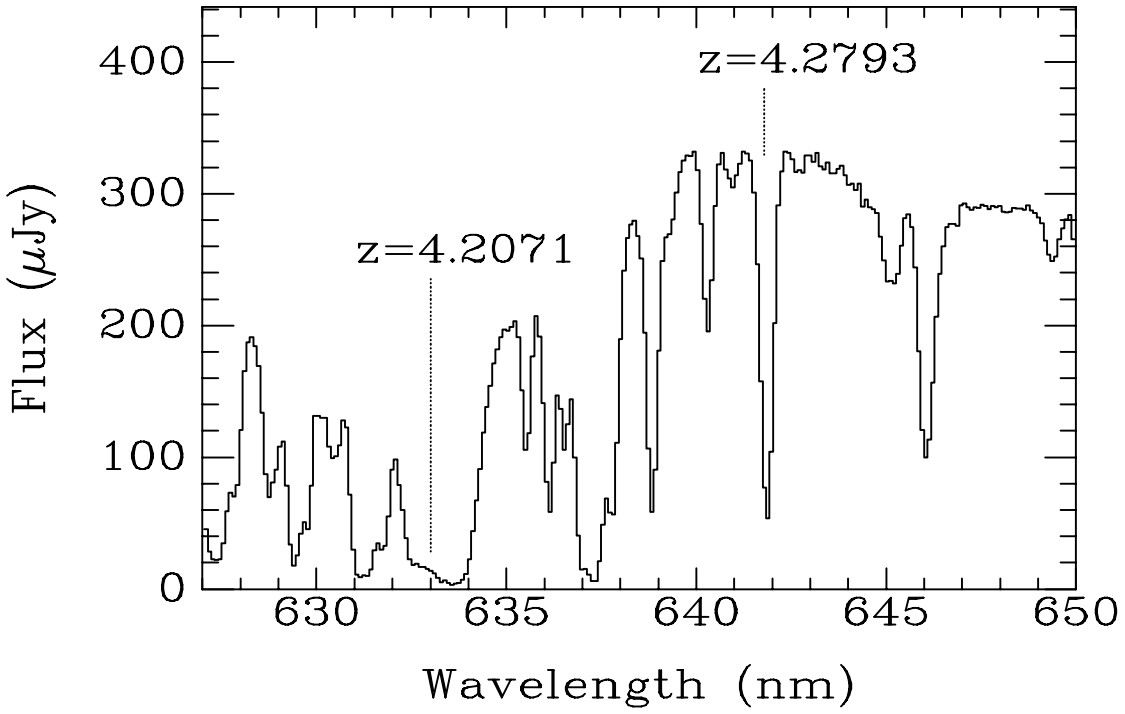


Figure 4. Close-up of the spectrum of QSO PSS 2155+1358, showing the wavelength of the main candidate Lyα emitter (z=4.2793), and of the second, more marginal detection (z=4.2071).

that we see the background QSO through the clouds implies that little dust is present.

We modeled the gas using version 06.02.09 of Gary Ferland's Cloudy photoionisation code (Ferland et al. 1998). The absorbing sub-clumps were modeled as plane-parallel slabs of constant density gas, exposed to continuum emission with a typical QSO spectrum, normalised to the observed luminosity of PSS 2155+1358.

We place a lower limit on the ionisation parameter $U > 0.1$. This limit comes from our observed lower limit on the ratio of the C IV to C III column density, and is, to first order, independent of the density. No upper limit on U can be placed. The gas is therefore highly ionised: the fraction of hydrogen that is in the neutral state is $< 2\times10^{-5}$. While the measured neutral column density is only $4.7\times10^{15}\mathrm{cm}^{-2}$, the total ionised hydrogen column is more like that of a damped Lyman-α absorption-line system. For $U = 0.1$, we get a good fit to the observed column densities of both nitrogen and carbon if the metallicity is 6% (-1.2 dex) of solar. If the ionisation parameter is larger, we need carbon to be overabundant with respect to nitrogen - a trend which has been seen before in QSO spectra (eg. Hamann & Ferland 1999).

Each sub-clump reprocesses around 15% of incident ionising photons into Lyα photons. If most sight-lines through the cloud intersect a sub-clump (as suggested by the presence of three along the QSO sight-line), this means that the cloud must be around 50 Kpc from the QSO to have the luminosity observed. If it is further, an additional ionisation source would be required.

How big are the sub-clumps? If they are 50kpc from the QSO, and $U = 0.1$, the inferred gas density needed to give this ionisation parameter is $\sim 3\times10^{2}\mathrm{cm}^{-3}$. The total gas column is $\sim 10^{20}\mathrm{cm}^{-2}$, giving a sub-clump thickness of 3×10^{17}cm. If $U \sim 1$, the inferred density drops by a factor of ten and the ionised column increases by an order of magnitude, giving sub-clumps a hundred times as thick.

Thus if the absorbing gas is associated with the Lyα emitter, we're not looking at the host galaxy of the QSO. Instead, we are looking at an isolated cloud of metal-enriched gas many tens of kpc away, perhaps a satellite galaxy of the QSO host. If, however, the absorber is not connected with the emission, we have fewer constraints, and could be looking at gas closer in, the emission from which is suppressed by one of the mechanisms listed in the bullet points above.

If the emitter really is ~ 50 kpc from the QSO, as required if it is connected with the absorption line, then it is a little surprising that we see it at a projected separation of only $0.8''$ from the QSO. 50kpc in the plane of the sky would correspond to a separation of 8 arcsec. If emitters are distributed randomly within 50 kpc of the QSO, 28% would lie within our data cube, and only 2.5% would lie within one projected arcsec of the QSO. Thus if we saw anything, the odds of it being within $1''$ are $\sim 10\%$. This is not unlikely enough to rule anything out, but is curious and perhaps provides weak evidence that the emitter is closer to the QSO and hence not connected with the absorber.

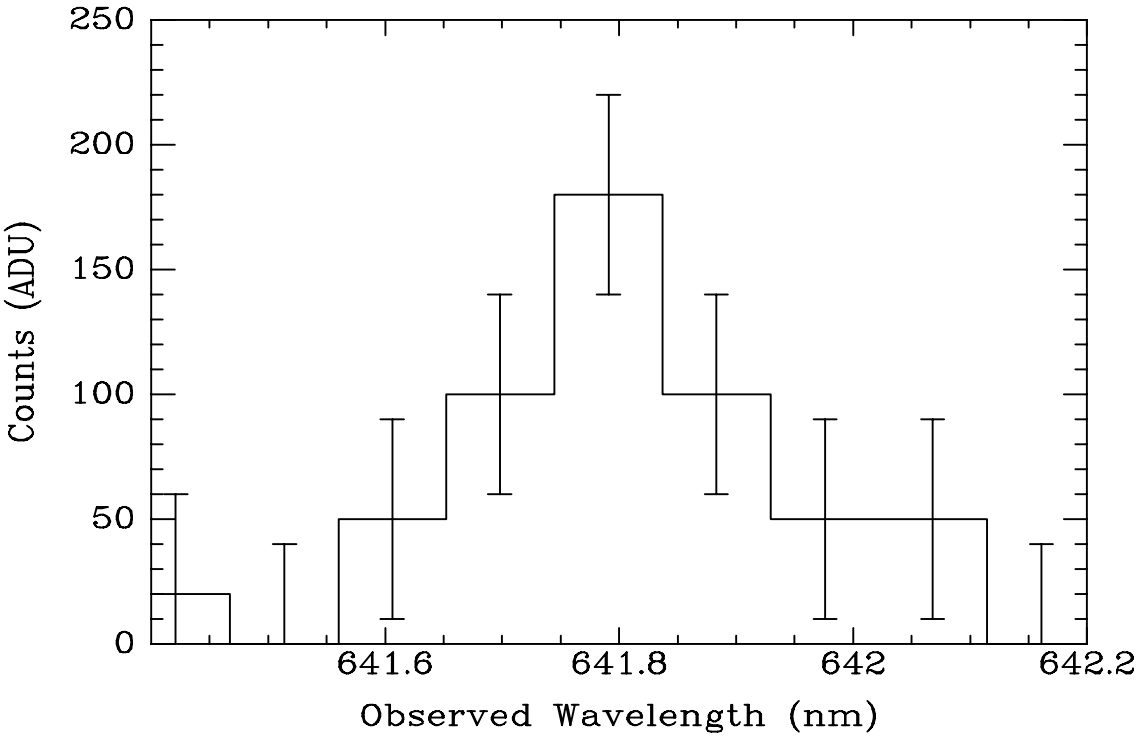


Figure 5. Spectrum of the candidate Lyα emission line at z=4.2793.

5 THE MARGINAL EMITTER AT REDSHIFT 4.2071

In addition to the main emission-line at z=4.2793, a second, more marginal line is seen at z=4.2071 (Fig 7). This is located $\sim 0.8''$ west of the QSO, and has a flux of about 1.0×10^{-17}erg cm^{-2}s^{-1}. It too is spectrally unresolved. Formally, it is significant at about the 6σ level, but it is too faint to see clearly in the data from individual nights, and hence could be some sort of glitch in the data.

This emitter lies in the blue wing of a sub-Damped-Lymanα absorption-line system in the QSO spectrum (Fig 4). This absorption system was studied by Dessauges-Zavadsky et al. (2003) and consists of two components, at redshifts of 4.212229 and 4.212628. If the existence of this emitter is confirmed, and if it is indeed associated with this nearby absorber, it would join the small number of such absorption-line systems seen in emission (eg. Warren et al. 2001; Møller et al. 2002; Weatherley et al. 2003; Kulkarni et al. 2006, and refs therein).

6 CONCLUSIONS

Perhaps our most striking conclusion is how little neutral gas lies close to QSO PSS 2155+1358. We detect one isolated cloud, which is probably $\sim$ 50kpc from the QSO. But there is no extended Lyα nebula, as seen around radio galaxies, radio-loud QSOs and in Lyα blobs. The emission we do detect is much fainter than that seen by Weidinger, Møller & Fynbo (2004) and Bunker et al. (2003). Clearly the properties of gas around high redshift QSOs are diverse.

ACKNOWLEDGMENTS

Based on observations obtained at the Gemini Observatory, which is operated by the Association of Universities for Research in Astronomy, Inc., under a cooperative agreement with the NSF on behalf of the Gemini partnership: the National Science Foundation (United States), the Particle Physics and Astronomy Research Council (United Kingdom), the National Research Council (Canada), CONICYT (Chile), the Australian Research Council (Australia), CNPq (Brazil) and CONICET (Argentina). The program number was GN-2004B-Q-21. Data from the European Southern Observatory's Very Large Telescope were also used. We'd like to thank Céline Peroux for making available the reduced UVES spectrum of PSS 2155+1358.0

REFERENCES

Adelberger, K.L., Steidel, C.C., Kollmeier, J.A. & Reddy, N.A. 2006, ApJ 637, 75
Alam, S.M.K. & Miralda-Escudé, 2001, ApJ 568, 576
Barkana, R. & Loeb, A. 2003, Nature, 421, 341
Bremer, M.N., Fabian, A.C., Sargent, W.L.W., Steidel,

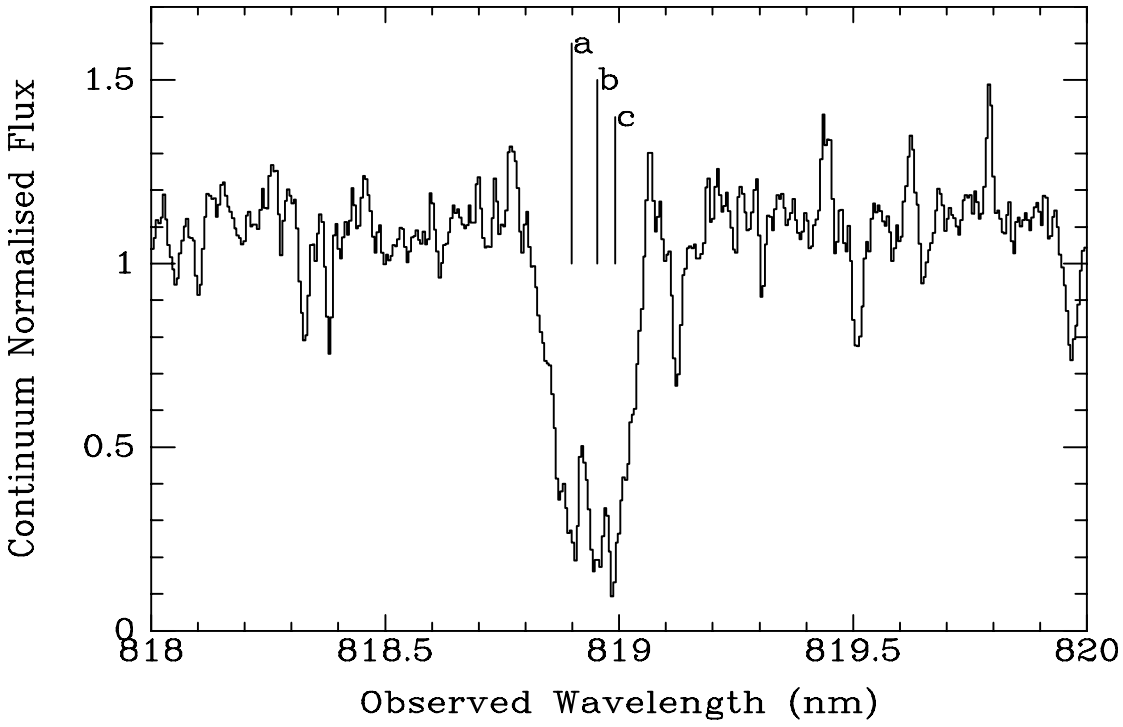


Figure 6. The UVES spectrum of the CIV (155.077 nm) absorption-line, showing the three components.

C.C., Boksenberg, A. & Johnstone, R.M. 1992, MNRAS 258, P23
Bunker, A., Smith, J., Spinrad, H., Stern, D. & Warren, S. 2003, Astrophys. Space Sci. 284, 357
Bunker, A.J., Marleau, F.R. & Graham, J.R. 1998, AJ, 116, 2086
Cantalupo, S., Porciani, C., Lilly, S.J. & Miniati, F. 2005, ApJ, 628, 61
Colbert, J.W., Teplitz, H., Francis, P.J., Palunas, P., Williger, G.M. & Woodgate, B.E. 2006, ApJL, 637, L89
Dessauges-Zavadsky, M., Péroux, C., Kim, T.-S., D'Odorico, S. & McMahon, R.G. 2003, MNRAS, 345, 447
Ferland, G.J., Korista,K.T., Verner,D.A., Ferguson, J.W., Kingdon, J.B. & Verner, E.M. 1998, PASP, 110, 761
Francis, P.J. & Bland-Hawthorn, J.B. 2004, MNRAS, 353, 301
Francis, P.J., Nelson, B.O. & Cutri, R.M. 2004, Aj 127, 646
Francis, P.J., Hewett, P.C., Foltz, C.B., & Chaffee, F.H. 1992, ApJ 398, 476
Francis, P.J., Hewett, P.C., Foltz, C.B., Chaffee, F.H., Weymann, R.J. & Morris, S.L. 1991, ApJ, 373, 465
Francis, P.J. et al. 2001, ApJ 554, 1001
Furlanetto, S.R., Schaye, J., Springel, V. & Hernquist, L. 2003, ApJL, 599, L1
Gould, A. & Weinberg, D.H. 1996, ApJ, 468, 462
Haiman, Z. & Rees, M.J. 2001, ApJ, 468, 87
Hamann, F. & Ferland, G. 1999, ARAA, 37, 487
Heckman, T.M., Lehnert, M.D., Miley, G.K. & van Breugel, W. 1991, ApJ, 381, 373
Hogan, C.J. & Weymann, R.J. 1987, MNRAS, 225, P1
Hu, E.M., Cowie, L.L. & McMahon, R.G. 1998, ApJL, 502, L99
Hu, E.M., McMahon, R.G. & EGami, E. 1996, ApJL, 459, L53
Kulkarni, V.P., Woodgate, B.E., York, D.G., Thatte, D.G., Meiring, J., Palunas, P. & Wassell, E. 2006, ApJ 636, 30
Mar, D.P., & Bailey, G. 1995, PASA, 12, 239
Matsuda, Y. et al. 2004, AJ, 128, 569
Møller, P. & Warren, S.J. 1993, A&A, 270, 43
Møller, P., Warren, S.J. & Fynbo, J.U. 1998, A&A, 330, 19
Møller, P., Warren, S.J., Fall, S.M., Fynbo, S.M. & Jakobsen, P. 2002, ApJ 574, 51
Péroux, C., Storrie-Lombardi, L.J., McMahon, R.G., Irwin, M. & Hook, I.M. 2001, AJ 121, 1799
Venemans, B.P., Kurk, J.D., Miley, G.K., Röttgering, H.J.A., van Breugel, W., Carilli, C.L., Ford, H., Heckman, T., McCarthy, & Pentericci, L., 2002, A&A, 361, 25
Warren, S.J., Møller, P., Fall, S.M. & Jakobsen, P. 2001, MNRAS, 326, 759
Weatherley, S.J., Rawwen, S.J., Møller, P., Fall, S.M., Fynbo, J.U. & Croom, S.M. 2003, MNRAS, 358, 985
Weidinger, M., Møller, P. & Fynbo, J.P.U., 2004, Nature, 430, 999

This paper has been typeset from a TEX/ LATEX file prepared by the author.

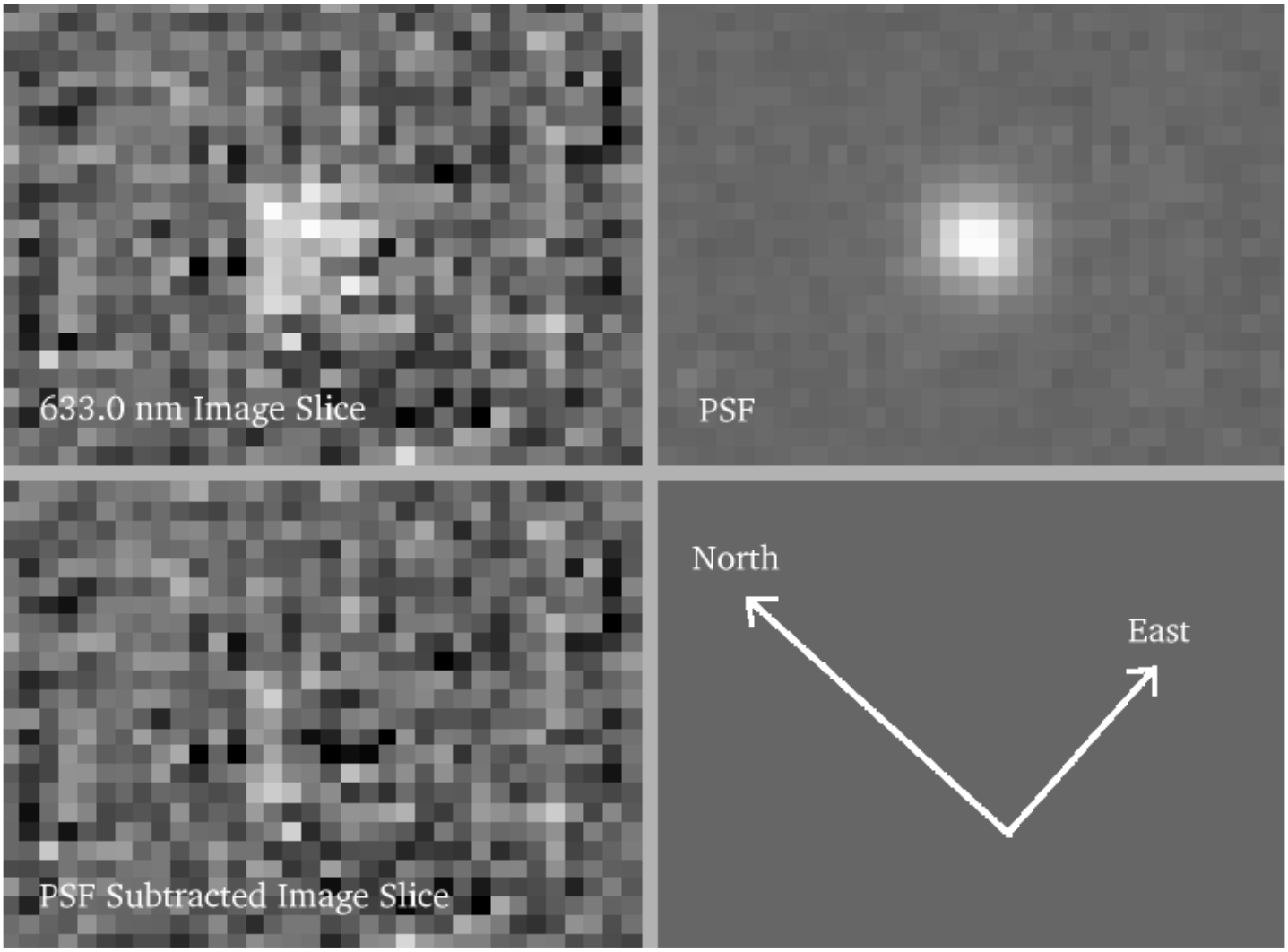


Figure 7. The candidate Lyα emitter at reshift 4.2071. The top left panel shows a single spatial slice through the data cube at 630.00nm wavelength. The point spread function generated from other slices near this wavelength is shown in the top right panel. The bottom left panel shows the PSF subtracted image. The candidate emitter lies below and to the left of the QSO. Each image is $7''$ wide and $5''$ high. Upwards in the images corresponds to $50°$ east of north on the sky.